Nanoscale

RSC Publishing

PAPER

View Article Online
View Journal | View Issue



Cite this: *Nanoscale*, 2013, **5**, 2511

# Polyoxometalate-stabilized, water dispersible $Fe_2Pt$ magnetic nanoparticles†

K. M. Seemann,*[abc] A. Bauer,[a] J. Kindervater,[a] M. Meyer,[d] C. Besson,[ce] M. Luysberg,[f] P. Durkin,[g] W. Pyckhout-Hintzen,[d] N. Budisa,[g] R. Georgii,[ab] C. M. Schneider[c] and P. Kögerler[ce]

Received 29th October 2012
Accepted 16th January 2013

DOI: 10.1039/c3nr33374d

www.rsc.org/nanoscale

Magnetic $Fe_2Pt$ core–shell nanoparticles with 2 nm cores were synthesized with a monolayer coating of silicotungstate Keggin clusters. The core–shell composition is substantiated by structural analysis performed using high-resolution scanning transmission electron microscopy (HR-STEM) and small angle X-ray scattering (SAXS) in a liquid suspension. The molecular metal oxide cluster shell introduces an enhanced dispersibility of the magnetic Fe–Pt core–shell nanoparticles in aqueous media and thereby opens up new routes to nanoparticle bio-functionalization, for example, using pre-functionalized polyoxometalates.

## Introduction

Nanoparticles have attracted enormous attention due to a wealth of novel physical effects and material properties expected to occur in reduced dimensions. The new possibilities opened up by nanoparticle-based composite materials, so-called nanocomposites or nanomaterials,[1–6] are most promising, especially in view of the combination of manifold properties, such as luminescence or fluorescence and magnetic properties.[7–11] On the other hand, nanoscale particles may pose a potential risk to human health and the environment when released in an uncontrolled manner.[12] The interaction between nanoscale, colloidal particles and biological cells may be diverse, but has remained largely unknown up to now.[13,14] Both the solubility in aqueous solutions induced by a coating shell[15,16] and the surface chemistry of nanoparticles play a crucial role with respect to their biological activity. For example, carboxylated Fe–Pt nanoparticles and Fe–Pt nanoparticles decorated by proteins such as transferrin or human serum albumin that are both abundant in blood serum, have been shown to enter HeLa cancer cells.[17] While these findings propose biofunctionalized nanoscale particles as carriers for targeted drug delivery or other biomedical applications such as *in vivo* imaging of tumors,[18,19] caution has to be exercised to prevent nanoscale particles from accidentally entering healthy cells by pinocytosis. This non-specific form of endocytosis leads to the inclusion of nanoparticles of diameters up to several hundred nanometers into the interior of a cell and may possibly cause unwanted mutagenesis due to specific nanoparticle toxicity.[20]

In view of these criteria it is desirable to investigate inorganic, molecular coatings to magnetic core nanoparticles, since they offer completely different surface chemical properties in addition to their magnetism.

The cytotoxicity aspects of nanoscale particles are an important additional feature that characterizes their compatibility for biomedical applications. The cytotoxicity of metallic nanoparticles depends on the core and critically on the shell composition. This is shown in the work of N. Lewinski *et al.*,[21] which summarizes the cytotoxicity of various kinds of nanoparticles to human dermal fibroblasts and a range of other cells. The average loss of viability determined from assay tests by chemical reduction of the dye 3-(4,5-dimethylthiazol-2-yl)-2,5-diphenyltetrazoliumbromide (MTT) is generally based on 24 hour exposures of fibroblast cells to nanoparticle suspensions of concentrations ranging from 0 to 1000 μg $L^{-1}$ inside well-plates. While bare super-paramagnetic iron-oxide nanoparticles of a diameter of 50 nm lead to a loss of cell viability of 25–50% in MTT tests, a coating of the same iron-oxide nanoparticles by polyethyleneglycol (PEG) reduced the toxicity considerably, leaving 99% of the exposed cells viable.[22] These findings were utilized successfully for the transfer of iron oxide nanoparticles

[a]*Physik Department E21, Technische Universität München, D-85748 Garching, Germany. E-mail: Klaus.Seemann@frm2.tum.de; k.seemann@fz-juelich.de*

[b]*Forschungsneutronenquelle Heinz Maier-Leibnitz, Technische Universität München, D-85748 Garching, Germany*

[c]*Peter Grünberg Institute (PGI-6) and JARA-FIT, Research Centre Jülich, D-52425 Jülich, Germany*

[d]*Jülich Centre for Neutron Science (JCNS-1) and Institute for Complex Systems (ICS-1), Research Centre Jülich, D-52425 Jülich, Germany*

[e]*Institut für Anorganische Chemie, RWTH Aachen University, D-52074 Aachen, Germany*

[f]*Peter Grünberg Institute (PGI-5), Ernst-Ruska Centre for Microscopy and Spectroscopy with Electrons, Research Centre Jülich, D-52425 Jülich, Germany*

[g]*Institut für Organische Chemie, Technische Universität Berlin, D-10585, Berlin, Germany*

† Electronic supplementary information (ESI) available: Details of materials, methods and experiments. See DOI: 10.1039/c3nr33374d

to the aqueous dispersion by introducing organic hydrophilic compounds to the surface yielding a high biocompatibility at the same time.[23]

Beyond the organic compounds such as amino silanes[24] and dextrans[25] used for coating and functionalization of magnetic nanoparticles, a wide variety of core–shell nanoparticles have been synthesized on a chemical route or deposited onto solid substrates by physical deposition methods. These core–shell nanoparticles have mostly been of bi-metallic nature, often with transition metal cores and noble metal shells. Elemental gold for example is a popular shell material used for iron, cobalt, nickel and manganese nanoparticle cores as it is chemically inert and is highly biocompatible. Elemental silver, platinum and palladium have also been used to coat transition metal nanoparticles.[26] Ferromagnetic FePt nanoparticles have been synthesized utilizing a FePt–MgO core–shell morphology[27] or a $FePt/Fe_3O_4/MgO$ structure.[28] The MgO coating of the FePt core prevents sintering of nanoparticles during the high temperature phase transition from the superparamagnetic to the ferromagnetic phase and secondly yields a hydrophilic nanoparticle surface that enables water dispersibility.

For this work we use polyoxometalates as coating molecules, a choice motivated by their high thermodynamic stability, their well-established potential to stabilize metallic (noble metal) nanoparticles and the fact that this class of compounds and their derivates have lately been considered for their anticancer properties.[29] Another advantage of polyoxometalates is that their solubility in various media can be tuned by exchange of the associated cations. This opens up possibilities to adjust the degree of water solubility of a metallic nanoparticle when coated by polyoxometalates with different cations.[30–32] Here we follow the approach of exchanging the potassium cations of the monolacunary silicotungstate Keggin polyanion $\alpha$-$[SiW_{11}O_{39}]^{8-}$ by long chain alkylammonium cations (trimethyl-hexadecyl-ammonium = TMHDA). The solubility of this salt in non-polar organic solvents allows a one-pot synthesis of silicotungstate-coated iron–platinum binary alloy particles by reduction of iron and platinum precursors. We carry out a detailed structural characterization by infrared spectroscopy (IR), high resolution scanning transmission electron microscopy (HR-STEM) in combination with energy dispersive X-ray analysis (EDX) and small angle X-ray scattering (SAXS) directly performed in a liquid suspension. Additionally, we show data of the magnetic properties, *i.e.* magnetization field scans at low temperatures and magnetization *vs.* temperature scans to provide evidence of the superparamagnetic behavior of the silicotungstate coated iron–platinum particles. All investigations were performed in relation to non-coated Fe–Pt nanoparticles prepared under identical conditions.

## Experimental work: nanoparticle synthesis and characterization

The reduction of platinum(II) and iron(II) acetylacetonate precursors by hexanediol at 280 °C in dioctyl ether in the presence of oleyl amine and oleic acid produces well-defined Fe–Pt nanoparticles.[33] Introduction of the polyoxometalate $[SiW_{11}O_{39}]^{8-}$ (=$\{SiW_{11}\}$) in the reacting medium allows the formation of Fe–Pt nanoparticles coated with a shell of polyoxotungstate anions. The resulting structure is schematized in Fig. 1(a).

Infrared spectroscopy is a well-suited method to analyse polyoxometalates due to their pronounced characteristic vibrational bands. The coated core–shell nanoparticles show strong IR bands between 500 and 1000 $cm^{-1}$, which are typical for silicotungstates with a Keggin structure.[34] This confirms the expected stability of the polyoxometalate framework under the core–shell nanoparticle synthesis conditions. The comparison of the spectrum with that of the precursor $TMHDA_{7.3}K_{0.2}H_{0.5}$-$[SiW_{11}O_{39}]$ (= TMHDA-$\{SiW_{11}\}$) illustrated in Fig. 1(b) shows a modification of the spectrum. The narrowing or fusion of the bands, coupled with a shift to higher wavenumbers, is characteristic of the formation of a complete Keggin structure which can be formulated as $[SiW_{11}O_{39}M(OH_2)]^{n-}$, wherein M denotes a metal atom. Iron(II) is known to easily coordinate to lacunary polyoxometalates such as $\{SiW_{11}\}$.[35] On the other hand, the usual square-planar coordination geometry of platinum(II) renders its incorporation in $\{SiW_{11}\}$ unlikely. We therefore assign the polyoxometalate actually present at the Fe/Pt surface to $[SiW_{11}O_{39}Fe^{II}(OH_2)]^{6-}$, which readily oxidizes to $[SiW_{11}O_{39}Fe^{III}(OH_2)]^{5-}$ (= $\{SiW_{11}Fe\}$) under ambient conditions. The additional bands observed in the spectrum of the $\{SiW_{11}Fe\}$–$Fe_2Pt$ core–shell particles can be attributed to the organic cations present with the polyoxometalate. Uncoated Fe–Pt nanoparticles reveal only the weak bands of the oleyl amine (OY) and oleic acid (OA).

The elemental analysis of $\{SiW_{11}Fe\}$–$Fe_2Pt$ nanoparticles indicates a Fe/W/Pt ratio of $2.1 \pm 0.2/1.3 \pm 0.2/1$. Assuming that all tungsten is present as $\{SiW_{11}Fe\}$, this yields a stoichiometry of $Fe_2Pt$ for the metallic nanoparticle core. In the absence of polyoxometalates, the reaction results in an $Fe_3Pt$ composition. In both cases, this corresponds to a limited incorporation of platinum with respect to the stoichiometry of the precursors. Marked differences between the stoichiometries of the starting

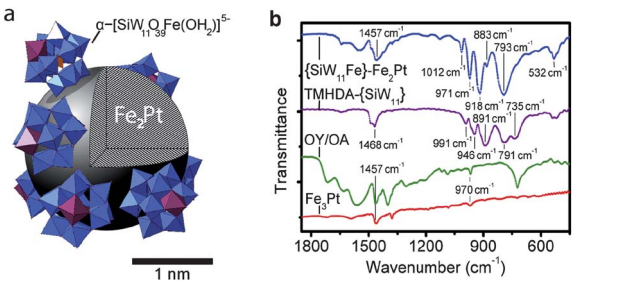


**Fig. 1** (a) Schematic representation of the core–shell structure of the $\{SiW_{11}Fe\}$–$Fe_2Pt$ particles. The spherical nanoparticle is covered by iron-incorporating Keggin polyoxometalates $[SiW_{11}O_{39}Fe(OH_2)]^{5-}$ ($FeO_6$ octahedra, purple; $WO_3$ octahedra, blue; $SiO_4$ tetrahedra, orange). (b) Infrared spectra of non-coated (red) and core–shell $Fe_3Pt$ nanoparticles (blue) reveal vibrational modes between 500 and 1000 $cm^{-1}$ characteristic for Keggin-type polyoxometalates. The infrared spectrum of the initial TMHDA-ligated Keggin polyoxometalates (purple) is shown for comparison together with the representative mixture of oleic acid (OA) and oleyl amine (OY) (green) serving as the surfactant during the metal nanoparticle synthesis.

 

materials and the resulting nanoparticles have already been observed by Liu and coworkers.[33] The introduction of the lacunary silicotungstate $\{SiW_{11}\}$ and the subsequent incorporation of part of the iron in its structure favors the formation of nanoparticles with increased platinum content (see ESI† for more details).

## The core–shell morphology of the nanoparticles

In order to gain more insight into the morphology of the core–shell nanoparticles we perform aberration-corrected, high-resolution scanning transmission electron microscopy (HR-STEM) to directly image the shape, size and crystallinity of the core crystallite. Since the contrast in the high resolution high-angle annular dark field (or *Z*-contrast) images (Fig. 2(a) and (b)) scales approximately with the square of the atomic number $Z^2$, Fe–Pt particles show bright contrast in comparison to the thin Si support film (see ESI† for details on the preparation). In both images some of the particles reveal the lattice plane contrast of the face-centered cubic phase, indicating their crystalline nature. For the core–shell $Fe_2Pt$ nanoparticles seen in Fig. 2(a) the lattice planes measure 2.2 Å in distance, in accordance with the value observed for bulk samples with a similar stoichiometry. The particles clearly display a surrounding shell, *i.e.* the core nanocrystals are enclosed by a weak-contrast rim. Within this rim, some brighter dots appear, which arise from individual, heavy atoms and which we attribute to W. One such individual W atom is marked by an arrow. The average diameter of the core–shell particles is 2.3 ± 0.3 nm, that is $[Fe_2Pt]_{160\pm60}$. Given the W/Pt ratio determined by elemental analysis, this yields a $[Fe_2Pt]_{160}[SiW_{11}O_{39}Fe(OH_2)]_{20}Q_{100}$ stoichiometry ($Q^+ = TMHDA^+$, oleyl ammonium). Nearly 30 $\{SiW_{11}Fe\}$ molecules with a diameter of 1.2 nm are the geometrical limit of packing the surface of the 2.3 nm diameter spherical $Fe_2Pt$ core particle, which corresponds to a surface coverage of *ca.* 80%.[36] While the presence of organic cations such as $Q^+$ balances the electrostatic repulsion between the $\{SiW_{11}Fe\}$ polyanions, sterically they may also prevent a higher surface coverage closer to the geometrical limit. From elemental analysis we estimate 20 molecules per individual core–shell nanoparticle corresponding to a surface coverage of 60% with $\{SiW_{11}Fe\}$. The surface of the core–shell $Fe_2Pt$ nanoparticles is notably irregular and rugged while the overall shape of the particles in general has a spherical appearance. Since the $\{SiW_{11}Fe\}$ shell is prone to radiation damage, we abstain from determining an overall outer diameter for the core–shell nanoparticles from HR-STEM results.

In comparison, the non-coated $Fe_3Pt$ nanoparticles shown in Fig. 2(b) are of larger average diameter, *i.e.* 3.1 ± 0.2 nm, are noticeably faceted and exhibit a distance of neighboring lattice planes of 2.0 Å. The increased lattice parameter of core–shell *vs.* non-coated nanoparticles is due to the larger stoichiometric content of Pt in the core–shell $Fe_2Pt$ nanoparticles compared to the non-coated $Fe_3Pt$ nanoparticles. The surface of the $Fe_3Pt$ nanoparticles is well-defined and does not show the presence of the scattering centers in the immediate vicinity of the nanoparticle observed in the case of the core–shell nanoparticles. Additionally, we are able to confirm the main elemental constituents of the core–shell nanoparticles for an ensemble of some 20 nanoparticles using energy dispersive X-ray analysis (EDX) that combines with the lateral resolution of the TEM images. Fig. 2(c) shows a typical EDX spectrum obtained from $\{SiW_{11}Fe\}$–$Fe_2Pt$ core–shell nanoparticles. Signals characteristic for binding energies of tungsten (W Lα, W Lβ), platinum (Pt Mβ, Pt Kα, Pt Lβ) and iron (Fe Kα) are detected, which are the elements present in the $\{SiW_{11}Fe\}$ shell to the $Fe_2Pt$ nanoparticles. The signal attributed to elemental silicon as another constituent of the molecular shell could not be distinguished from the substrate peak of the Si membrane TEM sample carrier and therefore the EDX spectrum in Fig. 2(c) shows only the peaks relevant to the core–shell $\{SiW_{11}Fe\}$–$Fe_2Pt$ nanoparticles. Since the overall diameter of the core–shell nanoparticles is not accessible by HR-STEM we resort to an additional experimental technique, *i.e.* SAXS carried out in a liquid suspension.

A conclusive description of the morphology of the core–shell nanoparticles including the polyoxometalate shell is obtained preferably in a liquid suspension. The physical mechanism of scattering a photon off the electron density of the shell molecules is ideally suited to gain more insight into the structure of the core–shell nanoparticles when combined with the STEM data. This holds especially for their diameters when considered in relation to the core crystallite diameter obtained from STEM experiments. The details of the data collection and experimental set-up used are described in ESI.† In Fig. 3(a) the scattering

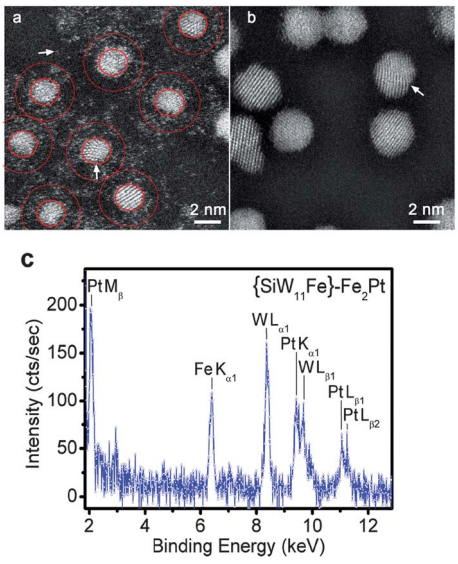


**Fig. 2** HR-STEM images of the core–shell $Fe_2Pt$ particles (a) indicate a shell surrounding each of the particles of core diameter 2.3 nm caused by the polyoxotungstate clusters. The core and shell are delineated by pairs of concentric circles for clarity. Individual, heavy atoms within the shell can be identified by their bright, dot-like contrast, the arrow in the upper left quarter marks one of these atoms. All particles are crystalline. The particles in (a) and (b) marked with an arrow consist of two crystalline domains. For comparison, non-coated $Fe_3Pt$ particles with a diameter of 3.1 nm are shown in (b). The elemental composition of the core–shell particles determined by TEM-EDX analysis (c) on an ultrathin Si-membrane reveals the three heavy atomic species tungsten (W), platinum (Pt) and iron (Fe).

curves of our two different nanoparticle samples in a dilute liquid suspension are shown. The scattered X-ray photon intensity $I(q)$ is related to the scattering vector $q = 4\pi \sin(\Theta)/\lambda$ and the radius of gyration in $I(q) = I_0 e^{-(qR_g)^2/3}$ in the case $qR_g \lesssim 1$.[37] The scattering angle is defined as $2\Theta$ and $\lambda$ is the wavelength of the Cu K$\alpha$ line. Due to the limited size of the particles the Guinier law is appropriate. ln *I versus* $q^2$ as shown in the inset of Fig. 3(a) linearizes the scattering curve. The linear slope is a direct measure of the radius of gyration and can easily be extracted. In the case of homogeneous, monodisperse spheres, as witnessed by HR-STEM for our nanoparticles, the diameter is calculated from the radius of gyration $R_g$ according to $D = 2\sqrt{\frac{5}{3}}R_g$. For the non-coated $Fe_3Pt$ nanoparticles a diameter of 3.8 ± 0.5 nm is obtained, which is slightly larger than the average diameter of 3.1 ± 0.2 nm determined by HR-STEM.

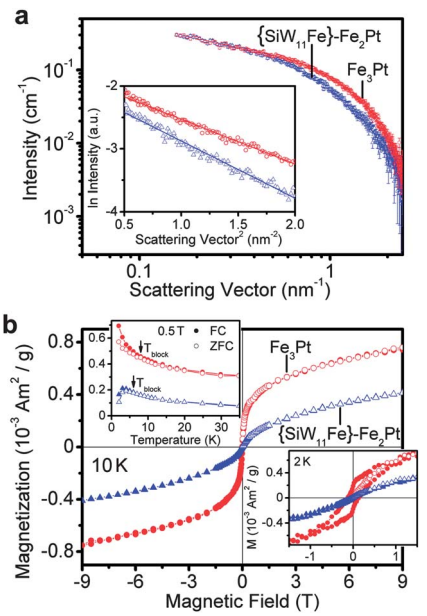


**Fig. 3** (a) SAXS curves (NanoStar, Bruker AXS) of the $\{SiW_{11}Fe\}$–$Fe_2Pt$ core–shell nanoparticles (blue data points) and the non-coated $Fe_3Pt$ nanoparticles (red data points) obtained from a liquid suspension in hexane solvent yield an overall particle diameter of approximately 4.8 nm for the core–shell $Fe_2Pt$ nanoparticles compared to an average particle diameter of 3.8 nm in the non-coated $Fe_3Pt$ sample. The logarithmic plot (inset) of the scattered X-ray intensity *vs.* the squared scattering vector linearizes the scattering data (open symbols). The solid line represents the Guinier fit to the data points resulting in larger particle diameters in the coated sample (blue) compared to the non-coated particles (red). (b) At $T$ = 10 K, the field-dependent magnetization of both the $\{SiW_{11}Fe\}$–$Fe_2Pt$ (blue) and the non-coated $Fe_3Pt$ (red) nanoparticles shows superparamagnetic behaviour. The relative magnetic moment (open symbols represent the virgin branch) is notably reduced for $\{SiW_{11}Fe\}$–$Fe_2Pt$ to nearly half of the value found for the non-coated $Fe_3Pt$ particles (red). The inset in the upper left corner illustrates the evolution of the magnetization with decreasing temperature for both, the core–shell $Fe_2Pt$ and the non-coated $Fe_3Pt$ sample for the zero-field-cooled (ZFC, open symbols) and field-cooled (FC, filled symbols) measurements: the $Fe_3Pt$ nanoparticles exhibit a blocking temperature of $T_{block}$ = 8 K, the $\{SiW_{11}Fe\}$–$Fe_2Pt$ core–shell $T_{block}$ = 6 K. The magnetization-field scans at $T$ = 2 K (inset in the lower right corner) show the onset of hysteresis for the $\{SiW_{11}Fe\}$–$Fe_2Pt$ core–shell nanoparticles while the $Fe_3Pt$ particles are clearly ferromagnetic and have a notably larger coercivity than the core–shell nanoparticles.

This is attributed to the organic ligands OY and OA used to disperse the purified nanoparticles in *n*-hexane to form a liquid suspension. The ligands can form a thin shell around the individual nanoparticles and thus give an additional scattering contrast. The diameter obtained for the $\{SiW_{11}Fe\}$–$Fe_2Pt$ core–shell nanoparticles on the other hand is 4.8 ± 0.5 nm, which is significantly larger than the diameter of 2.3 ± 0.3 nm found for the $Fe_2Pt$ core crystallite in the HR-STEM experiments. This method-specific discrepancy in diameters is unambiguously assigned to the polyoxometalate shell present in the core–shell nanoparticles containing heavy atoms. Taking the core–shell character of the $\{SiW_{11}Fe\}$–$Fe_2Pt$ nanoparticles into account, the overall radius of gyration can be related to a core radius and a shell thickness[38] *via* $R_g^2 = \frac{3}{5}R_o^2 + \frac{1}{(\overline{\rho} - \rho_m)V}\left[\frac{3}{5}(\rho_i - \overline{\rho})R_i^2 V_i + (\rho_o - \overline{\rho})R_{g,o}^2 V_o\right]$ with the overall nanoparticle volume $v = (4\pi/3)R_o^3$. The average electron density $\overline{\rho} = \frac{V_i\rho_i + V_o\rho_o}{V}$ is given by the individual electron densities of the core $\rho_i$, the shell $\rho_o$ and the medium of suspension $\rho_m$ with corresponding volumes of the core crystallite $v_i = (4\pi/3)R_i^3$ and shell $v_o = (4\pi/3)(R_o^3 - R_i^3)$, while the radius of gyration for the shell is defined as $R_{g,o}^2 = \frac{3}{5}\frac{(R_o^5 - R_i^5)}{(R_o^3 - R_i^3)}$. We analyze the core–shell morphology of the $\{SiW_{11}Fe\}$–$Fe_2Pt$ nanoparticles by taking the diameter $2R_i$ determined from HR-STEM as a fixed parameter along with the electron density of the $Fe_2Pt$ core and the $\{SiW_{11}Fe\}$ shell molecule. Thereby, we are able to extract a shell thickness of 1.2 ± 0.3 nm formed by the polyoxometalate which is in excellent agreement with the size of the $\{SiW_{11}Fe\}$ cluster anion of 1.2 nm. This is conclusive evidence of the core–shell morphology in the $\{SiW_{11}Fe\}$–$Fe_2Pt$ nanoparticles and proof of the effectiveness of our chemical route to polyoxometalate coated Fe–Pt nanoparticles.

## Magnetic properties

The magnetic properties of the $\{SiW_{11}Fe\}$–$Fe_2Pt$ core–shell nanoparticles in comparison to the non-coated $Fe_3Pt$ nanoparticles are examined by conventional low temperature magnetometry (see ESI† for details). A shift in the stoichiometric content of Fe within the core crystallite from iron-rich $Fe_3Pt$ for the non-coated nanoparticles to $Fe_2Pt$ in the core–shell nanoparticles is the main motivation for magnetometric measurements, as the magnetic moment is expected to be considerably reduced for the core–shell nanoparticles containing one-third less Fe than the non-coated ones. The magnetization *versus* field scans were recorded for the core–shell nanoparticles as well as for the non-coated nanoparticles for applied magnetic fields of up to ±9 Tesla and temperatures ranging from 300 K to 2 K. The samples were measured in their as-made state, *i.e.* no annealing procedure at elevated temperatures was carried out. After cooling to the measurement temperature in zero-field we recorded the magnetization-field scans as shown for $T$ = 10 K in Fig. 3(b). Both, core–shell and non-coated nanoparticles show superparamagnetic behavior at this temperature. At an applied magnetic field of $\mu_0 H$ = 9 Tesla

 

the magnetic moment of the {$SiW_{11}Fe$}–$Fe_2Pt$ core–shell nanoparticles yield a magnetization of $M_{\text{core–shell}} \approx 4.0 \times 10^{-4}$ $Am^2\ g^{-1}$ and account for approximately only half of the value for the non-coated $Fe_3Pt$ nanoparticles for which we find $M_{\text{non-coated}} \approx 8.0 \times 10^{-4}$ $Am^2\ g^{-1}$. The difference in specific magnetization is mainly explained by two mechanisms. First, the non-magnetic {$SiW_{11}Fe$} molecular shell lowers the magnetically relevant mass fraction in the nanoparticle sample. Second, the Fe content in the $Fe_2Pt$ crystallite of the core–shell nanoparticle is reduced as compared to the non-coated $Fe_3Pt$ particles. The blocking temperature of the magnetic nanoparticles, generally defined as $T_{\text{block}} = \frac{K \cdot V}{k_B \cdot \ln\left(\frac{\tau_m}{\tau_0}\right)}$, wherein $K \cdot V$ accounts for the magneto-crystalline anisotropy energy of the nanoparticle, represents an energy barrier for the random and thermally activated switching of the magnetic moment of the nanoparticles. This energy barrier is surpassed for measurement temperatures $T$ above $T_{\text{block}}$. The factor $\ln\left(\frac{\tau_m}{\tau_0}\right)$ relates the measurement time $\tau_m$ to the so-called attempt time $\tau_0$ characteristic for the material of the nanoparticle according to the Néel–Arrhenius equation. The blocking temperature of nanoparticles is strongly size-dependent and equi-stoichiometric core–shell FePt nanoparticles of an average core diameter of 5 nm and face-centered-cubic structure usually yield blocking temperatures of $T_{\text{block}} < 10$ K.[15] Depending on the product of $K \cdot V$, materials that show ferromagnetic behavior in macroscopic samples may become superparamagnetic at the nanoscale. Only very large anisotropy energy densities as known from the $L1_0$–FePt system of face-centered-tetragonal structure lead to ferromagnetism in macroscopic samples and nanoparticles alike.[11,39] We determine the blocking temperature of both nanoparticle systems by $M(T)$ measurements (left inset of Fig. 3(b)) and find for the $Fe_3Pt$ nanoparticles a blocking temperature of $T_{\text{block}} = 8$ K, while we find for the {$SiW_{11}Fe$}–$Fe_2Pt$ core–shell nanoparticles a lower blocking temperature of $T_{\text{block}} = 6$ K. This is mainly due to the smaller size and lower Fe content of the core–shell nanoparticles compared to the non-coated particles. The magnetization-field scans measured at $T = 2$ K, clearly below the blocking temperature of both systems, are shown in the lower right inset of Fig. 3(b) for both, the {$SiW_{11}Fe$}–$Fe_2Pt$ core–shell nanoparticles (coercivity $H_c = 40$ mT) and the $Fe_3Pt$ particles with a notably larger coercivity of $H_c = 130$ mT than the core–shell nanoparticles.

## Dispersibility in aqueous media and routes to nanoparticle functionalization

As motivated earlier, the use of nanoparticles in bio-imaging and drug delivery is of great interest to the scientific community. Having the ability to tune the physical or biocompatibility properties of the particles, such as fluorescence or solubility *in vivo*, simply by functionalizing the particles with the appropriate substrates is clearly a desirable goal. To showcase a potential application of the {$SiW_{11}Fe$}–$Fe_2Pt$ nanoparticles, a general method allowing the ligation of a wide array of substrates to the nanoparticles was sought. Peptides and proteins play a key role in cellular recognition, and so loading the nanoparticles with these types of compounds could allow for interesting biological applications.

The water-dispersibility of the magnetic Fe–Pt core–shell nanoparticles is introduced by the solubility of the original polyoxometalate in aqueous media. After the synthesis the oleyl amine and oleic acid ligands make the {$SiW_{11}Fe$}–$Fe_2Pt$ and $Fe_3Pt$ nanoparticles dispersible in *n*-hexane, but not water (Fig. 4(d) and (e)). We have tested the dispersibility of the Fe–Pt core–shell nanoparticles in ethanol (Fig. 4(a)) and de-ionized water (Fig. 4(b)) after removing the residual oleyl amine and oleic acid ligands by treatment in a Soxhlet extractor using *n*-heptane for 16 hours. The presence of the {$SiW_{11}Fe$} shell surrounding the $Fe_2Pt$ nanoparticles was subsequently verified by IR spectroscopy. The Fe–Pt core–shell nanoparticles were readily dispersible in de-ionized water and also pure ethanol (Fig. 5(I)) opening up routes to functionalization with organic compounds *via* the known methods of covalent grafting of polyoxometalate molecules.[40] The vacant site in polyoxometalates is of especially high relevance in this respect. Thorimbert and coworkers[41] have described reactions leading to carboxyl-polyoxometalates utilizing a carboxyl stannane insertion reaction involving the monovacancy of a Keggin-type polyoxometalate. This direct carboxylation of polyoxometalates can yield nanoparticle-POM scaffolds that are promising for the biological post-functionalization of the Fe–Pt core–shell nanoparticles described in the presented work (Fig. 5(II)). A classical amide coupling is the first choice for the ligation of peptides and bio-organic compounds with the nanoparticles. Explicit experiments to bio-functionalize the polyoxometalate coated Fe–Pt nanoparticles are beyond the scope of this work.

Experiments to carboxylate the {$SiW_{11}Fe$}–$Fe_2Pt$ core–shell nanoparticles *via* a ligand exchange reaction based on mercapto-undecanoate (MUA) following the description by H. G. Bagaria *et al.*[42] result in the core–shell nanoparticles being

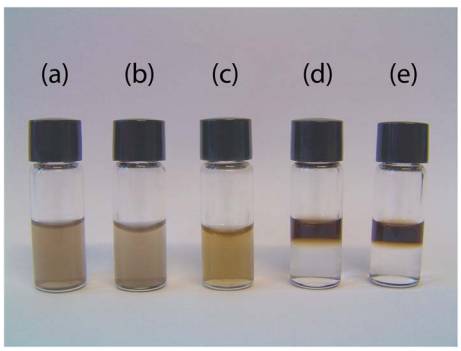


**Fig. 4** (a) {$SiW_{11}Fe$}–$Fe_2Pt$ nanoparticles free of the oleic acid and oleyl amine ligands dispersed in pure ethanol, (b) the same {$SiW_{11}Fe$}–$Fe_2Pt$ core–shell nanoparticles dispersed in de-ionized water, (c) carboxylated $Fe_2Pt$ nanoparticles dispersed in de-ionized water after treatment with mercapto-undecanoate. For comparison, the {$SiW_{11}Fe$}–$Fe_2Pt$ nanoparticles (d) and $Fe_3Pt$ nanoparticles (e) after synthesis disperse in *n*-hexane but not in de-ionized water, creating a clearly visible phase separation.

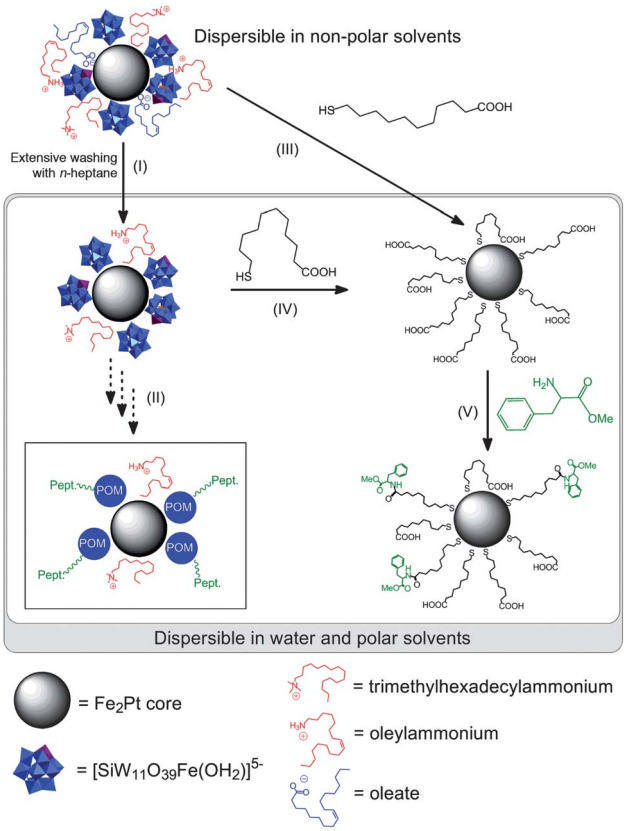


**Fig. 5** Schematic of the combination of nanoparticle shell and ligands to the $Fe_2Pt$ nanoparticles and their dispersibility properties, respectively. The $\{SiW_{11}Fe\}$–$Fe_2Pt$ core–shell nanoparticles in the as-made state are dispersed in the non-polar solvent *n*-hexane. Washing to remove the OA and OY ligands (I) yields dispersibility of the $\{SiW_{11}Fe\}$–$Fe_2Pt$ core–shell nanoparticles in water and polar solvents and are proposed for covalent grafting of the polyoxometalate to attach peptides *via* amide coupling reactions (II). Ligand exchange using mercapto-undecanoate (MUA) replaces the silicotungstate clusters (III and IV) as well as the OA and OY ligands. An amide coupling reaction using the amino acid phenylalanine (Phe) exemplifies the functionalization of the $Fe_2Pt$ nanoparticles (V).

stripped of their polyoxometalate shell in addition to the organic ligands oleic amine and oleyl acid (Fig. 5(III) and (IV)). The ligand exchange reaction using MUA (see ESI† for details) was verified by IR spectroscopy; however, the strong IR bands assigned to $\{SiW_{11}Fe\}$ were absent in the ligand exchanged core–shell nanoparticle sample. This also clarifies questions regarding the type of bonding of the $\{SiW_{11}Fe\}$ compound to the $Fe_2Pt$ core. The binding of the carboxyl group of MUA to Fe and the thiol group to Pt at the surface[42] of the $Fe_2Pt$ core is energetically more favorable than the chemisorption of the $\{SiW_{11}Fe\}$ to the core nanoparticle (Fig. 5(III) and (IV)).

The bio-functionalization of the bare $Fe_2Pt$ nanoparticles that were carboxylated by MUA and dispersible in de-ionized water (Fig. 4(c)) was exemplified directly by coupling of the nanoparticles with a bio-organic compound.

The ligation of an amino acid was chosen as a model system for this, specifically phenylalanine methyl ester (H-Phe-OMe) which was coupled *via* a classical peptide coupling reaction (Fig. 5(V); see ESI† for details of the amide coupling reaction). This amino acid derivative was selected as the reporter for this system as it possesses a characteristic UV-visible absorption maximum of H-Phe-OMe (~258 nm), which provides a spectrophotometric handle to indicate the ligation of the amino acid to the carboxylate functional groups of the MUA residues protruding from the surface of the nanoparticles. The measured UV-visible absorption profile of the unmodified mercapto-undecanoate FePt nanoparticles showed no significant absorption bands through the range of 250–500 nm, making H-Phe-OMe ideal as a reporter molecule. Indeed, after subjecting the carboxylated $Fe_2Pt$ nanoparticles to the coupling reaction an absorption maximum at 258 nm was unambiguously observed with a similar profile to that of the free amino acid (Fig. 6).

Further evidence to support the success of the coupling reaction would be the presence of a fluorescence signal associated with the amino acid residue. However, due to the poor fluorescence profile of phenylalanine (very low quantum yield 0.024)[43] a distinct fluorescence maximum was not observed. Despite this, the distinct UV-visible absorption more than makes up for this shortcoming, with the general principle of amide coupling being shown with success for the nanoparticles.

This enables us to postulate that the ligation of peptides, proteins or other moieties amenable to coupling reactions can be achieved in a similar fashion.

Regarding the cytotoxicity of bare FePt particles Kim and co-workers[44] have investigated the cell viability based on mouse brain endothelial cells (bEnd3) and found no significant toxicity for the non-coated FePt particles unless the cells were exposed to extremely high nanoparticle concentrations. The ligand exchange reaction using MUA introduces carboxyl groups to the surface of the nanoparticles and is a phase transfer similar to the one described by W. W. Yu and coworkers,[23] which in turn is not expected to raise any cytotoxicity of the FePt nanoparticles used for functionalization with biochemical compounds such as phenylalanine. The amino acid phenylalanine serves as an example for biological ligands that are used for

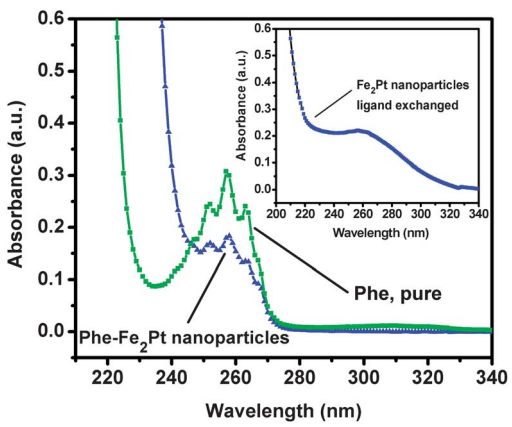


**Fig. 6** Measured UV-Vis spectrum of the mercapto-undecanoate ligand exchanged $Fe_2Pt$ nanoparticles after coupling with the amino acid phenylalanine (blue) and reference spectrum of 5 mM phenylalanine H-Phe-OMe (green) dissolved in de-ionized water. The UV-Vis spectrum of the ligand exchanged $Fe_2Pt$ nanoparticles prior to coupling is shown in the inset. All spectra were measured in aqueous medium.

biofunctionalization of the nanoparticles towards biomedical applications. The phase-transfers of iron-oxide nanoparticles into an aqueous dispersion using a similar organic shell as we do with MUA, introducing carboxyl groups, has been shown to dramatically decrease any cytotoxicity of magnetic nanoparticles.[22,23] According to the observation that nanoparticle cytotoxicity decisively depends on the shell compounds,[21] the $\{SiW_{11}Fe\}$ silicotungstate shell molecules on the other hand should determine the toxicity of the $\{SiW_{11}Fe\}$–$Fe_2Pt$ core–shell nanoparticles. A thorough examination of the cell viability and cytotoxicity tests based on the exposure of human fibroblasts to $\{SiW_{11}Fe\}$–$Fe_2Pt$ will shed more light into the biocompatibility of this type of core–shell nanoparticles.

## Conclusions

We have shown a successful chemical route to synthesize the water dispersible core–shell $Fe_2Pt$ nanoparticles using the polyoxotungstate $\{SiW_{11}\}$, representing the first binary nanoparticles stabilized by polyoxometalates. Using a range of experimental methods such as FT-IR spectroscopy, HR-STEM, SAXS and magnetometry, we characterize size, morphology and magnetic properties of the Fe–Pt core–shell nanoparticles in comparison to Fe–Pt particles that were synthesized in an analogous manner, however, without the coating precursor additive. Hence, we are able to draw a conclusive picture of the $\{SiW_{11}Fe\}$–$Fe_2Pt$ core–shell nanoparticles. The vacancy of the Keggin-type polyoxotungstate is found to be occupied by an Fe atom to form $\{SiW_{11}Fe\}$ anions, which simultaneously reduces the stoichiometric content of Fe within the core crystallite particle from $Fe_3Pt$ in the non-coated case to $Fe_2Pt$ for the core–shell nanoparticles as verified by elemental analysis. This is consistent with a larger specific magnetic moment measured in non-coated $Fe_3Pt$ nanoparticles compared to the core–shell $Fe_2Pt$ nanoparticles. The nanoparticles are superparamagnetic and have a blocking temperature of $T_{block} = 6$ K in the case of the $\{SiW_{11}Fe\}$–$Fe_2Pt$ core–shell nanoparticles and a blocking temperature of $T_{block} = 8$ K in the case of the $Fe_3Pt$ nanoparticles as expected for magnetic particles of an average diameter of 5 nm or less, respectively.

The core–shell nanoparticles exhibit reasonable dispersion properties in de-ionized water, which is mediated by the water solubility of the polyoxometalate. The example of the $\{SiW_{11}Fe\}$–$Fe_2Pt$ core–shell nanoparticles opens up a promising route to use such nanoparticle systems as drug carriers with the advantage of a combined effect when polyoxometalates with anti-cancer properties are employed. While the magnetic properties of the core Fe–Pt nanoparticles are exploited for hyperthermia treatment, the molecular shell releasing its anti-cancer effect in the vicinity of the malignant tissue could lead to a synergistic effect. The core–shell nanoparticles free of oleyl amine and oleic acid disperse in water, which is a necessary requirement for the covalent grafting of the polyoxometalate for bio-functionalization. We have shown that a ligand exchange reaction by mercapto-undecanoate yields water dispersible carboxylated $Fe_2Pt$ nanoparticles free of the polyoxometalate shell. *Via* a classical peptide coupling reaction we attached the amino acid phenylalanine to the carboxylated nanoparticles, which was confirmed by UV-visible spectrometric data.

## Notes

The authors declare no competing financial interest.

## Acknowledgements

The authors thank B. Botar, D.E. Bürgler, H. Lippert and P. Böni for fruitful discussions and support. The technical assistance by K. Bickmann and M. Stranger is also gratefully acknowledged.

## References

1 D. K. Yi, S. T. Selvan, S. S. Lee, G. C. Papaefthymiou, D. Kundaliya and J. Y. Ying, Silica-coated nanocomposites of magnetic nanoparticles and quantum dots, *J. Am. Chem. Soc.*, 2004, **127**, 4990–4991.

2 S. Wang, C. Querner, T. Dadosh, C. H. Crouch, D. S. Novikov and M. Drndic, Collective fluorescence enhancement in nanoparticle clusters, *Nat. Commun.*, 2011, **2**, 364–372.

3 Y. Lin and R. G. Finke, Novel polyoxoanion- and $Bu_4N^+$-stabilized, isolable and redissolvable, 20–30 Å $I_{300-900}$ nanoclusters: the kinetically controlled synthesis, characterization and mechanism of formation of organic solvent-soluble reproducible size, and reproducible catalytic activity metal nanoclusters, *J. Am. Chem. Soc.*, 1994, **116**, 8335–8353.

4 P. J. Kulesza, M. Chojak, K. Karnicka, K. Miecznikowski, B. Palys, A. Lewera and A. Wieckowski, Network films composed of conducting polymer-linked and polyoxometalate-stabilized platinum nanoparticles, *Chem. Mater.*, 2004, **16**, 4128–4134.

5 C.-H. Jun, Y. J. Park, Y.-R. Yeon, J.-R. Choi, W.-R. Lee, S.-J. Ko and J. Cheon, Demonstration of a magnetic and catalytic Co@Pt nanoparticle as a dual-function nanoplatform, *Chem. Commun.*, 2006, 1619–1621.

6 A. Neyman, L. Meshi, L. Zeiri and I. A. Weinstock, Direct imaging of the ligand monolayer on an anion-protected metal nanoparticle through cryogenic trapping of its solution-state structure, *J. Am. Chem. Soc.*, 2008, **130**, 16480–16481.

7 H. Yu, M. Chen, P. M. Rice, S. X. Wang, R. L. White and S. Sun, Dumbbell-like bifunctional Au–$Fe_3O_4$ nanoparticles, *Nanoletters*, 2005, **5**, 379–382.

8 W. Shi, H. Zeng, Y. Sahoo, T. Y. Ohulchanskyy, Y. Ding, Z. L. Wang, M. Swihart and P. N. Prasad, A general approach to binary and ternary hybrid nanocrystals, *Nano Lett.*, 2006, **6**, 875–881.

9 Y.-S. Lin, S.-H. Wu, Y. Hung, Y.-H. Chou, C. Chang, M.-L. Lin, C.-P. Tsai and C.-Y. Mou, Multifunctional composite nanoparticles: magnetic, luminescent, and mesoporous, *Chem. Mater.*, 2006, **18**, 5170–5172.

10 N. Pazos-Pérez, Y. Gao, M. Hilgendorff, S. Irsen, J. Pérez-Juste, M. Spasova, M. Farle, L. M. Liz-Marzán and

M. Giersig, Magnetic-nobel metal nanocomposites with morphology-dependent optical response, *Chem. Mater.*, 2007, **19**, 4415–4422.

11 C. Antoniak, M. E. Gruner, M. Spasova, A. V. Trunova, F. M. Römer, A. Warland, B. Krumme, K. Fauth, S. Sun, P. Entel, M. Farle and H. Wende, A guideline for atomistic design and understanding of ultrahard nanomagnets, *Nat. Commun.*, 2011, **2**, 528–535.

12 M. J. McCall, Nanoparticles in the real world, *Nat. Nanotechnol.*, 2011, **6**, 613–614.

13 C. Röcker, M. Plötzl, F. Zhang, W. J. Parak and G. U. Nienhaus, A quantitative fluorescence study of protein monolayer formation on colloidal nanoparticles, *Nat. Nanotechnol.*, 2009, **4**, 84–85.

14 I. Lynch, A. Salvati and K. A. Dawson, What does the cell see?, *Nat. Nanotechnol.*, 2009, **4**, 546–547.

15 D. C. Lee, F. V. Mikulec, J. M. Pelaez, B. Koo and B. Korgel, Synthesis and magnetic properties of silica-coated FePt nanocrystals, *J. Phys. Chem. B*, 2006, **110**, 11160–11166.

16 V. Mazumder, M. Chi, K. L. More and S. Sun, Core/shell Pd/FePt nanoparticles as an active and durable catalyst for the oxygen reduction reaction, *J. Am. Chem. Soc.*, 2010, **132**, 7848–7849.

17 X. Jiang, S. Weise, M. Hafner, C. Röcker, F. Zhang, W. J. Parak and G. U. Nienhaus, Quantitative analysis of the protein corona on FePt nanoparticles formed by transferrin binding, *J. R. Soc., Interface*, 2010, **7**, 5–13.

18 M. N. Rhyner, A. M. Smith, X. Gao, H. Mao, L. Yang and S. Nie, Quantum dots and multifunctional nanoparticles: new contrast agents for tumor imaging, *Nanomedicine*, 2006, **1**, 209–217.

19 X. Qian, X.-H. Peng, D. O. Ansari, Q. Yin-Goen, G. Z. Chen, D. M. Shin, L. Yang, A. N. Young, M. D. Wang and S. Nie, *In vivo* tumor targeting and spectroscopic detection with surface-enhanced Raman nanoparticle tags, *Nat. Biotechnol.*, 2008, **26**, 83–90.

20 A. M. Smith, H. Duan, A. M. Mohs and S. Nie, Bioconjugated quantum dots for *in vivo* molecular and cellular imaging, *Adv. Drug Delivery Rev.*, 2008, **60**, 1226–1240.

21 N. Lewinski, V. Colvin and R. Drezek, Cytotoxicity of nanoparticles, *Small*, 2008, **4**(1), 26–49.

22 A. K. Gupta and S. Wells, Surface-modified superparamagnetic nanoparticles for drug delivery: preparation, characterization, and cytotoxicity studies, *IEEE Trans Nanobiosci.*, 2004, **3**, 66–73.

23 W. W. Yu, E. Chang, C. M. Sayes, R. Drezek and V. L. Colvin, Aqueous dispersion of monodisperse magnetic iron oxide nanocrystals through phase transfer, *Nanotechnology*, 2006, **17**, 4483–4487.

24 M. Ma, Y. Zhang, W. Yu, H. Shen, H. Zhang and N. Gu, Preparation and characterization of magnetic nanoparticles coated by amino silane, *Colloids Surf., A*, 2003, **212**, 219–226.

25 R. S. Molday and D. MacKenzie, Immunospecific ferromagnetic iron-dextran reagents for the labeling and magnetic separation of cells, *J. Immunol. Methods*, 1982, **52**, 353–367.

26 J. Wang and X. C. Zeng, Core–Shell Magnetic Nanoclusters, in *Nanoscale Magnetic Materials and Applications*, ed. J. P. Liu, E. Fullerton, O. Gutfleisch and D. J. Sellmeyr, Springer-Verlag, 2009.

27 J. Kim, Ch. Rong, J. P. Liu and S. Sun, Disperible ferromagnetic FePt nanoparticles, *Adv. Mater.*, 2009, **21**, 906–909.

28 J. Kim, Ch. Rong, Y. Lee, J. P. Liu and S. Sun, From core–shell structured FePt/$Fe_3O_4$/MgO to ferromagnetic FePt nanoparticles, *Chem. Mater.*, 2008, **20**, 7242–7245.

29 T. Yamase, Anti-tumor, -viral and -bacterial activities of polyoxometalates for realizing an inorganic drug, *J. Mater. Chem.*, 2005, **15**, 4773–4782.

30 Y. Wang, A. Neyman, E. Arkhangelsky, V. Gitis, L. Meshi and I. A. Weinstock, Self-assembly and structure of directly imaged inorganic-anion monolayers on a gold nanoparticle, *J. Am. Chem. Soc.*, 2009, **131**, 17412–17422.

31 Y. Wang and I. A. Weinstock, Cation mediated self-assembly of inorganic cluster anion building blocks, *Dalton Trans.*, 2010, **39**, 6143–6152.

32 L. S. Ott and R. G. Finke, Transition-metal nanocluster stabilization for catalysis: a critical review of ranking methods and putative stabilizers, *Coord. Chem. Rev.*, 2007, **251**, 1075–1100.

33 K. E. Elkins, T. S. Vedantam, J. P. Liu, H. Zeng, S. Sun, Y. Ding and Z. L. Wang, Ultrafine FePt nanoparticles prepared by the chemical reduction method, *Nano Lett.*, 2003, **3**, 1647–1649.

34 R. Thouvenot, M. Fournier, R. Franck and C. Rocchiccioli-Deltcheff, Vibrational investigations of polyoxometalates. 3. Isomerism in molybdenum(VI) and tungsten(VI) compounds related to the Keggin structure, *Inorg. Chem.*, 1984, **23**, 598–605.

35 F. Zonnevijlle, C. M. Tourné and G. F. Tourné, Preparation and characterization of iron(III)- and rhodium(III)-containing heteropolytungstates. Identification of novel oxo-bridged iron(III) dimers, *Inorg. Chem.*, 1982, **21**, 2751–2757.

36 J. H. Conway and N. J. A. Sloane, *Sphere Packings, Lattices and Groups*, Springer-Verlag, New York, 1999, vol. 290, see also http://www.research.att.com/~njas/packings.

37 A. Guinier, La diffraction des rayons X aux tres petits angles; application a l'etude de phenomenes ultramicroscopiques, *Ann. Phys.*, 1939, **12**, 161–237.

38 I. Markovic, R. H. Ottewill, D. J. Cebula, I. Field and J. F. Marsh, Small-angle neutron-scattering studies on non-aqueous dispersions of calcium-carbonate. 1. The Guinier approach, *Colloid Polym. Sci.*, 1984, **262**, 648–656.

39 K. M. Seemann, V. Baltz, M. MacKenzie, J. N. Chapman, B. J. Hickey and C. H. Marrows, Diffusive and ballistic current spin polarization in magnetron-sputtered $L1_0$-ordered epitaxial FePt, *Phys. Rev. B: Condens. Matter Mater. Phys.*, 2007, **76**, 174435.

 

40 A. Proust, R. Thouvenot and P. Gouzerh, Functionalization of polyoxometalates: towards advanced applications in catalysis and materials science, *Chem. Commun.*, 2008, 1837–1852.
41 S. Thorimbert, B. Hasenknopf and E. Lacôte, Cross-linking organic and polyoxometalate chemistries, *Isr. J. Chem.*, 2011, **51**, 275–280.
42 H. G. Bagaria, E. T. Ada, M. Shamsuzzoha, D. E. Nikles and D. T. Johnson, Understanding mercapto ligand exchange on the surface of FePt nanoparticles, *Langmuir*, 2006, **22**, 7732–7737.
43 R. F. Chan, Fluorescence quantum yields of tryptophan and tyrosine, *Anal. Lett.*, 1967, **1**, 35–42.
44 D. K. Kim, D. Kan, T. Veres, F. Normadin, J. K. Liao, H. H. Kim, S.-H. Lee, M. Zahn and M. Muhammed, Monodispersed Fe–Pt nanoparticles for biomedical applications, *J. Appl. Phys.*, 2005, **97**, 10Q918.